Theor Chem Acc (2012) 131:1253
DOI 10.1007/s00214-012-1253-4

REGULAR ARTICLE

Mechanism of ketone hydrosilylation using NHC–Cu(I) catalysts: a computational study

Thomas Vergote · Thomas Gathy · Fady Nahra · Olivier Riant · Daniel Peeters · Tom Leyssens

Received: 29 March 2012 / Accepted: 23 June 2012 / Published online: 13 July 2012

Abstract The plausibility of the catalytic cycle suggested for the hydrosilylation of ketones by (NHC) copper(I) hydrides has been investigated by a theoretical DFT study. Model systems yield the necessary insight into the intrinsic reactivity of the system. Computations show the activation of the copper fluoride pre-catalyst, as well as both steps of the catalytic cycle to involve a 4-center metathesis transition state as suggested in the literature. These results show the reaction to be favored by the formation of van der Waals complexes resembling the transition states. Stabilizing electrostatic interactions between those atoms involved in the bond-breaking and bond-forming processes induces the formation of these latter. Both steps of the actual catalytic cycle show a free energy barrier of about 14.5 kcal/mol for the largest NHC ligands, with respect to the isolated reactants, hereby confirming the plausibility of the suggested cycle. The large overall exothermicity of the catalytic cycle of about 35 kcal/mol is in agreement with experimental observations.

Keywords N-heterocyclic diaminocarbene · Copper(I) · DFT · Hydrosilylation · Reactivity · Catalysis

Published as part of the special collection of articles celebrating theoretical and computational chemistry in Belgium.

Electronic supplementary material The online version of this article (doi:10.1007/s00214-012-1253-4) contains supplementary material, which is available to authorized users.

T. Vergote · T. Gathy · F. Nahra · O. Riant · D. Peeters · T. Leyssens (✉)
Institute of Condensed Matter and Nanosciences, Université Catholique de Louvain, Place Louis Pasteur 1, 1348 Louvain-la-Neuve, Belgium
e-mail: tom.leyssens@uclouvain.be

1 Introduction

Carbonyl bond reduction, specifically of aldehydes and ketones, to the corresponding alcohol functionality via hydride transfer is a fundamental transformation in organic synthesis [1–5]. Transition metal catalysis has been successfully applied in the reduction of many carbonyl compounds via hydrogenation or hydrosilylation [1–5]. Hydrogenation reactions often proceed in good yields but require high pressure or elevated temperature. Moreover, if the reaction is part of a multistep synthesis, the resulting free alcohol often requires protection prior to the next synthetic step. In contrast, the softer reactions conditions of hydrosilylation turned out to be a major advantage, in addition to the fact that both the reduction and the protection steps are performed in a single, atom-efficient step.

The first catalytic hydrosilylation systems, based on rhodium, were developed in the early 1970s [6–8]. Traditionally, catalytic hydrosilylation of the carbonyl functionality was performed with precious, heavy metals ranging from Re, Rh, and Ru to Ir [9–18]. As the main drawback of these systems is the cost affiliated with these metals, during the two last decades efforts were taken in finding an efficient alternative system using less-expensive metals such as titanium [19–26], iron [27–29], manganese [30, 31], or zinc [32–35]. In 1984, Brunner and Miehling reported the first asymmetric hydrosilylation using a copper-diphosphine catalyst [36]. Since many copper-diphosphine catalytic systems were developed [37–43], the active species formed in situ was postulated to be a copper (I) hydride. Lipshutz and co-worker describe the formation of the CuH species in a system combining a catalytic quantity of CuCl/NaOt–Bu/diphosphine and a stoichiometric quantity ofhydrosilylating agent [44–48]. At the same time, Carreira et al. [49], as well as Riant et al. [41, 50–52],

reported CuF_2 systems as interesting precursors to copper hydride. Based on these results, Wu et al. [53] recently developed a highly asymmetric copper(II)-catalyzed hydrosilylation system.

N-Heterocyclic carbene (NHC) ligands [54–57], particularly of the type developed by Arduengo et al. [58], have emerged as efficient ligands in metal-mediated reactions [59–62]. Compared to tertiary phosphines, the NHC ligands are characterized by strong metal–ligand bonding, hereby minimizing ligand dissociation [54–57]. This latter is particularly interesting when performing mechanistic studies, as this will simplify the system under study. NHC ligands were shown to be interesting alternatives to phosphines for the copper-catalyzed hydrosilylation of carbonyl compounds. While (IPr)–CuCl (IPr = 1,3-bis(2,6-diisopropylphenyl)imidazol-2-ylidene) was an efficient catalyst for the hydrosilylation of unhindered ketones [63], (ICy)–CuCl (ICy = 1,3-bis(cyclohexyl)imidazol-2-ylidene) or (SIMes)-CuCl (SIMes = 1,3-bis(2,4,6-trimethylphenyl) imidazolin-2-ylidene) turned out to be effective for more challenging ketones [64]. The active species, formed in situ in the presence of a catalytic amount of NaOtBu and a stoichiometric quantity of hydrosilylating agent, is a copper(I) hydride. Yun et al. [65] reported that the use of copper(II) salts as catalytic precursor in combination with a NHC also leads to an effective hydrosilylation of ketones. Recently, a series of cationic bis-carbenic complexes, $[(NHC)_2–Cu]X$ (X = BF_4^- [66, 67], PF_6^- [66, 67], FHF^- [68]), has shown remarkable activity toward the hydrosilylation of ketones. Although, once more, the reaction pathway was not investigated, mono-carbenic intermediates are believed to be the active species. Interestingly, the first asymmetric (NHC)copper(I)-catalyzed ketone hydrosilylation was only developed recently by Gawley et al. [69].

In all of the above-mentioned studies, the suggested mechanism is based on the catalytic cycle shown in Scheme 1 [43, 64, 68, 70, 71], illustrated using a (NHC)copper(I) chloride complex. As the Cu–Cl bond cannot be cleaved in an efficient manner by a hydride source (such as silane), the complex needs to be activated through ligand exchange, replacing chlorine with an alkoxide or a fluoride. As stated in our previous work [68], depending on the reaction conditions, addition of a mild source of fluoride (NEt_3·3HF) can lead to either a (NHC)Cu–F complex or a (NHC)Cu–FHF bifluoride complex. The copper(I) (bi)fluoride complexes are then expected to be activated through a σ-bond metathesis reaction with a silane to yield the desired copper(I) hydride catalyst, thought to be the active species [72]. This active species is then postulated to react with a ketone passing through a four-center transition state to form a copper alkoxide (*step 1*). Finally, the copper alkoxide undergoes a

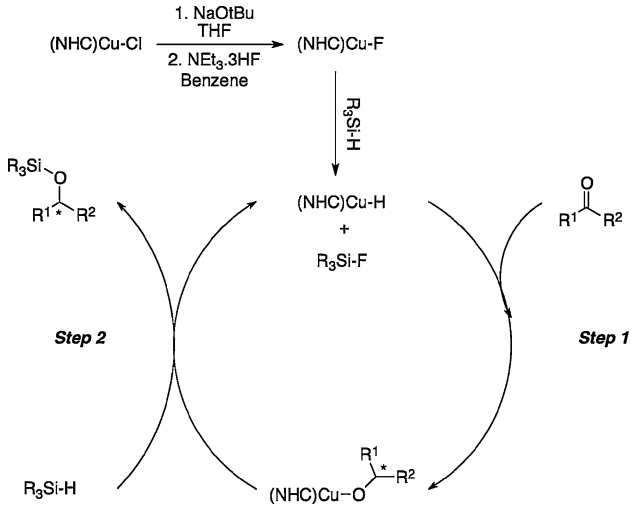

Scheme 1 Suggested cycle for the asymmetric hydrosilylation of ketones using (NHC) copper(I) catalysts

σ-bond metathesis with the hydrosilylating agent to regenerate the Cu–H complex and form the silylether product (*Step 2*). Although it has been suggested that (NHC)Cu–H species agglomerate in solution [73], no experimental evidence of this agglomeration in solution is available. However, this would imply that the equilibrium between monomeric and polymeric species is of prime importance for a complete understanding of the system under study. In this work, we do not investigate this aspect of the reaction, as it will only determine the final amount of free catalytic species available for catalysis but not the nature of the catalytic cycle itself.

This mechanism is relatively similar to the one proposed for the hydrosilylation of ketones catalyzed by phosphine copper(I) complexes [39, 42, 43]. Although some computational studies concerning the hydrosilylation reaction of ketones using copper(I) diphosphine complexes have been reported in the literature [74–78], surprisingly, no such studies have been reported for (NHC)–Cu(I) complexes. As these complexes are more stable compared to diphosphine Cu(I) complexes, and hence are interesting from a mechanistic point of view, it is important to compare their overall reactivity with the diphosphine complexes, to verify if the plausibility of the suggested catalytic cycle still stands, and to highlight possible differences. In this paper, we use computational chemistry to verify the plausibility of the suggested cycle, investigating energetic, electronic, and structural properties. Differences in the diphosphine complexes will also be highlighted.

Our calculations were made on models of increasing complexity, ranging from the simplest acyclic NHC ligand ("ADC_H") to the experimentally used unsaturated NHC ligands (shown in Scheme 2). Using a variety of NHC ligands, their effect on the catalytic cycle is studied. As our

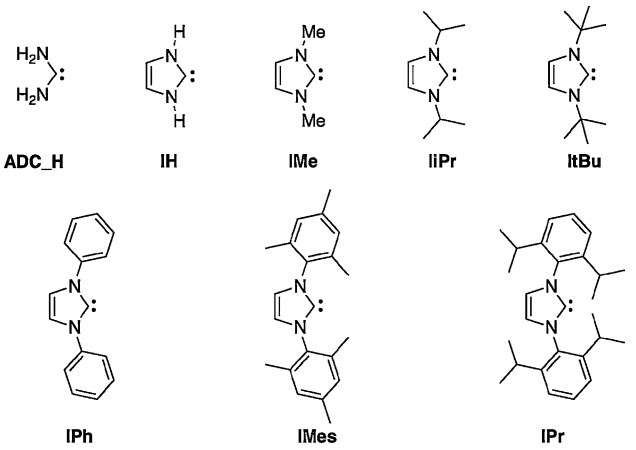

Scheme 2 Structure and acronyms of NHC ligands used throughout this work

first goal is to verify the plausibility of the catalytic cycles, as well as the effect of the NHC ligand, other reactants are modeled using formaldehyde and SiH_4 as model for, respectively, the ketone and silane species. The effect of a variation in ketone nature and silane nature could be studied at later stages, but goes beyond the scope of this contribution.

2 Computational details

Unless stated otherwise, all structures were fully optimized using Becke's three-parameter exchange functional [79] and the correlation functional of Lee, Yang, and Parr (B3LYP) [80], as implemented in the Gaussian 03 [81] series of programs. All possible conformations have been investigated and the most stable conformer is retained. Optimized geometries are provided as Supplementary material. Force constants were determined to characterize the stationary points, as well as to determine their entropies and free energies, based on a statistical thermodynamics treatment. For the transition state (TS), the correctness of the curvature and its corresponding eigenvector were checked in order to guarantee the quality of the obtained results. Accordingly, in some cases, intrinsic reaction coordinate (IRC) calculations were made to confirm the transition state corresponded to the actual reaction mechanism [82–85]. Reactants were allowed to interact on the potential energy surface (PES) and formed a van der Waals (VDW) intermolecular pre-reaction complex. van der Waals interaction energies should be taken as indicative, as DFT methods do not correctly account for dispersion interactions [86]. The Cu atom was described using an effective core potential to represent all but the valence n*d* and $(n + 1)s$ and outer core n*s* and *np* electrons [87–89]. The latter were described with a triple zeta contraction of the original double zeta basis set, and this combination is referred to as the LANL2DZ basis set. All non-metal atoms were described using the diffused and polarized 6-31 ++G(d,p) basis set [90, 91]. Natural bond orbitals (NBO) analysis was used to investigate electronic properties and charge distributions [92–95]. Density difference drawings were made using GAUSSVIEW [96]. Orange and blue zones indicate, respectively, an increase and decrease in electron density. Isodensity surfaces are shown at 0.01 e^-/Bohr^3 for Figs. 2 and 8 and at 0.005 e^-/Bohr^3 for Fig. 5.

To examine the basis set dependence, calculations using a larger basis set, 6-311G(2d,p) for all non-metal atoms and a def2-TZVP [97] basis set for Cu, were made using the (IMes)Cu-X model system. Results (Table S3 in the Supporting material) show a consistent shift up to 4 kcal/mol for all species involved in the transformation of the pre-catalyst, and of about 3 kcal/mol for the second step of the catalytic cycle, while almost no effect is observed for the first step. While these shifts do not change the energy ordering of the reactions paths, keeping the overall discussion unaltered, they are due to a basis set superposition error involving the fluorine and silicon atoms. The BSSE for the (IMes)Cu–F/SiH_4 and (IMes)Cu–OCH_3/SiH_4 complexes is a mere 1.0 kcal/mol using the LANL2DZ/6-31 ++G(d,p) basis set, but increases to 3.5 kcal/mol for these complexes using the def2-TZVP/6-311G(2d,p) (See Supporting Info, Table S1). This effect is no longer observed for the first step of the catalytic cycle, the BSSE for the (IMes)Cu–H/H_2CO system being a mere 0.3 kcal/mol with the def2-TZVP/6-311G(2d,p) basis set (instead of 0.9 kcal/mol for the LANL2DZ/6-31 ++G(d,p) basis set). This important BSSE for the CuF species can be reduced when introducing diffuse basis functions on the F and Si atoms.[1] Indeed, single-point calculations on the (IMes)Cu-X system with the all electrons def2-TZVP/6-311 ++G(2d,p) basis set show the basis set dependence on the whole catalytic cycle being negligible. As the main objective of this paper is to study the plausibility of the actual catalytic cycle, with the possibility of transposing the basis set used to larger systems in order to study the enantioselectivity, the smaller basis set was chosen throughout this work. To further check the reliability of our results, we have also decided to make additional calculations on the (IMes)Cu-X system using the pure GGA functional BP86 [98], and the B3PW91 [79, 99, 100] and MPW1PW91 [101] hybrid functionals, as these three were also proven effective for transition metal chemistry [102–104]. Results of single-point

[1] The BSSE contributes to an overestimation of the stabilization of these complexes with respect to isolated reactants. Excluding this contribution, the van der Waals complexes remain stabilized with respect to isolated reactants, and the overall discussion therefore remains unaltered.

calculations obtained with these functionals did not affect either the relative ordering of the reaction paths or the conclusions drawn from the energy ordering of the structures (i.e., consistent results with B3LYP). These numbers are therefore discussed in the Supporting Information only (Table S2). Finally, as concerns could arise because no polarization function is included in LANL2DZ, while polarization is taken into account for all non-metal atoms, single-point calculations were also made with the LANL2TZ(f) [89, 105, 106] basis set for Cu, which uses *f* polarization functions developed by Frenking's group [106]. In addition, we compared our results to the Stuttgart RSC 1997 (SDD) RECP [107–109] that contains an *f* function for the first-row transition elements. Once more, basis set dependence was found negligible (Table S3).

3 Results and discussion

The different parts of the catalytic cycle will be discussed separately, starting with a discussion on the activation of the pre-catalyst, followed by an investigation of the two steps of the actual catalytic cycle.

3.1 Activation of the pre-catalyst

Once the pre-catalyst formed, this species reacts with a hydrosilane via a σ bond metathesis reaction to yield the active copper hydride species. As shown in Scheme 3, the formation of a σ bond between the copper and hydrogen atoms occurs through transmetalation [46, 72, 110] passing by a 4-center transition state.

Table 1 shows the relative energy, enthalpy, and free energy of the van der Waals complexes and transition states. The reaction is guided by the initial formation of an energetically favored van der Waals complex between the pre-catalyst and the SiH_4 hydrogenating agent.

The electrostatic interaction between the negatively charged fluorine atom and the positively charged copper atom, as well as the interaction between the negatively charged hydrogen atom and the positively charged silicon atom (Table S4), most likely explains the driving force for the formation of this complex.

As expected for a σ bond metathesis, the transition states are characterized by increased Cu–F and Si–H bond lengths, while Cu–H and Si–F bonds become shorter. Investigation of how the electronic density changes upon the formation of the transition state can help to clarify the actual reaction mechanism. Figure 2 shows the differential density between, respectively, the transition state and the sum of both reactants at transition-state geometry. As shown in this figure, the transition state is characterized by a strong decrease in electron density around the copper atom, and a strong increase between the Si and F atoms, corresponding to the breaking of the Cu–F bond, in favor of the formation of the Si–F bond. The formation of the copper hydride bond and breaking of the Si–H bond can also be observed, but seem less advanced. The 4-center σ bond metathesis should therefore be characterized as an asynchronous concerted reaction, with the breaking of the Cu–F bond (or formation of the Si–F bond) being slightly more advanced than the transfer of the silicon-linked hydrogen atom to the copper atom.

To get a more quantitative measurement of synchronicity/asynchronicity, Wiberg indexes [111] and NBO bond orders (B_i) were calculated. B_i were computed using the NBO program as implemented in Gaussian 03, and the synchronicity (S_y) was estimated using the concept proposed by Moyano et al. [112–114] (for more details, see section V in the Supporting information).

Bond indexes were calculated for the four bonds involved in the σ-bond metathesis reaction, meaning Cu–F, Cu–H, Si–H, and Si–F bonds (Fig. 2); all other bonds remain practically unaltered during the process (Fig. 1).

Calculating Wiberg indexes B_i for reactant complexes, TS, and products complexes allows locating the position of the TS between reactant and product (Table 2). For simplicity, only results for NHC = ADC_H, IH, and IMes are shown in Table 2 as these are representative of the entire set of species studied (See Supporting material, Table S5–S7).

Table 2 shows that the Cu–F bond has disappeared up to approximately 90 % at the TS, while this is a mere 44 % for the Si–H bond. In parallel, the Si–F bond has formed to an extent of 67 %, whereas the Cu–H bond has barely been formed (38 %). A similar observation is made for all studied NHC ligands, leading to synchronicity values of $S_y = 0.78$–0.80, which is in agreement with the structural

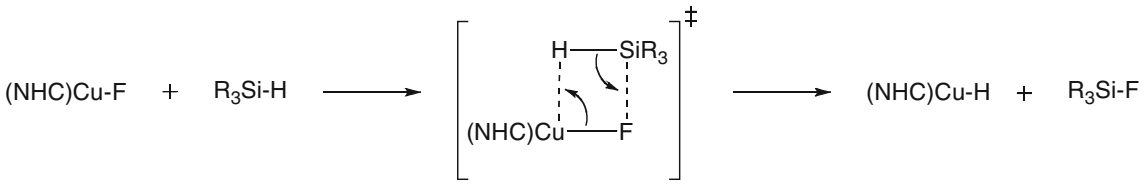

Scheme 3 Activation of the pre-catalyst

Table 1 Relative energy ΔE, enthalpy, and free energy (ΔH; ΔG) with respect to reactants for the pre-catalyst activation reaction

Pre-catalyst	van der Waals complex	TS	van der Waals complex	Products
(ADC_H)Cu–F	−1.2 (0.0; 6.2)	5.7 (6.0; 17.2)	−3.8 (−3.2; 4.8)	0.3 (−0.3; −0.6)
(IH)Cu–F	−1.2 (0.1; 6.0)	5.8 (6.1; 17.0)	−4.3 (−3.6; 4.4)	0.5 (−0.1; −0.4)
(IMe)Cu–F	−1.4 (−0.1; 6.4)	6.0 (6.4; 17.5)	−1.2 (−0.6; 7.4)	0.9 (0.3; 0.1)
(IiPr)Cu–F	−1.4 (−0.2; 5.8)	6.3 (6.7; 17.2)	−1.0 (−0.3; 6.8)	1.0 (0.4; 0.1)
(ItBu)Cu–F	−1.5 (−0.3; 5.9)	7.3 (7.6; 17.8)	−0.7 (0.0; 7.1)	0.3 (−0.3; −0.4)
(IPh)Cu–F	−1.8 (−0.5; 6.7)	6.5 (6.9; 17.6)	−1.0 (−0.4; 7.0)	0.8 (0.2; −0.1)
(IMes)Cu–F	−1.7 (−0.4; 6.1)	6.4 (6.8; 17.6)	−0.5 (0.1; 9.0)	1.4 (0.7: −0.9)
(IPr)Cu–F	−1.6 (−0.3; 8.2)	6.6 (7.0; 18.8)	¯0.1 (0.6; 9.9)	1.1 (0.5; 0.2)

Values are given in kcal/mol

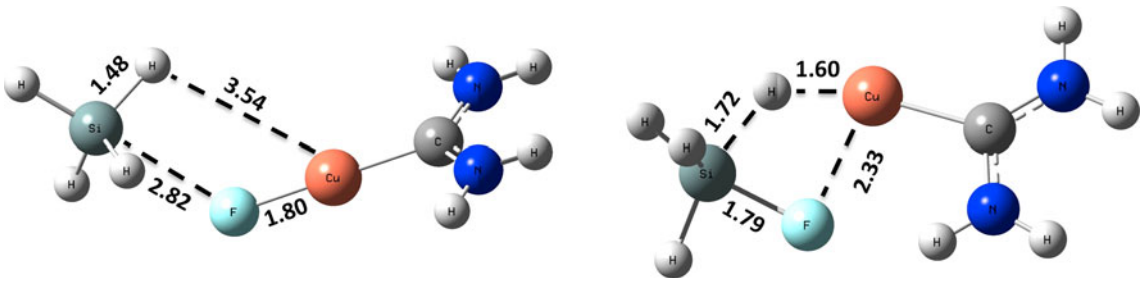

Fig. 1 Initial van der Waals complex and transition-state structure for the reaction between (ADC_H)Cu–F and SiH_4. Bond lengths are given in Å

Table 2 NBO analysis for the activation of the pre-catalyst

Pre-catalyst	Cu–F	Cu–H	Si–F	Si–H	δB_{AV}	S_y
(ADC_H)Cu–F						
B_i^R	0.2351	0.0011	0.0280	0.9473	0.597	0.79
B_i^{TS}	0.0250	0.2298	0.3548	0.5342		
B_i^P	0.0030	0.6084	0.5169	0.0017		
%Ev	90.52	37.66	66.84	43.69		
(IH)Cu–F						
B_i^R	0.2326	0.0011	0.0295	0.9471	0.599	0.78
B_i^{TS}	0.0225	0.2296	0.3552	0.5337		
B_i^P	0.0021	0.6159	0.5129	0.0061		
%Ev	91.15	37.17	67.38	43.93		
(IMes)Cu–F						
B_i^R	0.2170	0.0006	0.0327	0.9484	0.582	0.79
B_i^{TS}	0.0297	0.2107	0.3664	0.5523		
B_i^P	0.0028	0.5802	0.5371	0.0256		
%Ev	87.44	36.25	66.16	42.82		

Wiberg bond indexes (B_i), % evolution through the reaction coordinate ($\%E_v$), average bond index variation (δB_{AV}), and synchronicity parameters (S_y)

and electronic parameters (See Supporting material, Table S11), and confirms the qualitative interpretation shown in Fig. 2. As the Cu–F bond breaking ($\%E_v \approx 90\ \%$) is more advanced than all of the other bond changes at the transition state, the $Cu^{\delta+}$–$F^{\delta-}$ polarization of this bond is expected to be a determining factor in this reaction.

The activation reactions show a free energy barrier[2] of about 18 kcal/mol (Table 1). The more important barrier for the IPr NHC ligand can be explained by an increased steric effect around the copper atom. Table 1 confirms the

[2] Free energy barriers are reported with respect to isolated reactants.

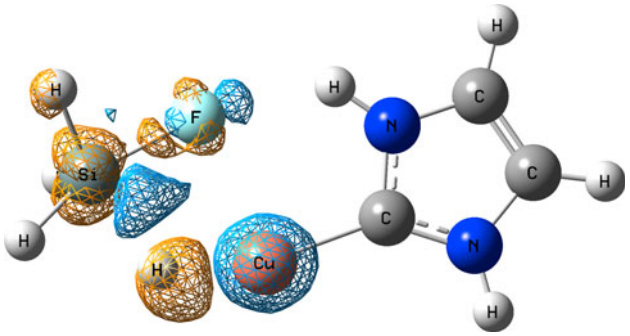

Fig. 2 Density difference between transition state and sum of reactants at transition-state geometry

importance of such a steric effect, showing a slight increase in free energy barrier when going from NHC = ADC_H to NHC = IMes.

These free energy barriers are relatively important, especially for a catalytic reaction, and in particular when compared to the ones obtained for diphosphines ligands [74]. The high barriers could be indicative of a different activation mechanism in solution. Calculations in solution on alternative mechanisms are currently ongoing.

The activation mechanism is nearly thermoneutral ($\Delta H = -0.3$–0.7 kcal/mol). As mentioned above, the fluorine atom is essential to the activation of the pre-catalyst, as other copper halogen complexes show little to no reactivity. Our results show that this observation is most likely due to the strong polarization of the Cu–F bond.

3.2 Catalytic cycle

Once activated, the copper hydride species enters the catalytic cycle. The proposed mechanism for the hydrogenation of ketones occurs through a two-step cycle as presented in Scheme 4. A first step concerns the formation of a copper alkoxide, through a σ metathesis similar to that observed for the activation of the pre-catalyst. In a second step, another 4-center transition state between this alkoxide and a hydrosilane leads to a silylated ether, and the reactivated catalyst. The alcohol can be recovered through hydrolysis of the silylated ether. Due to the fact the alkoxide complex is not observed experimentally, the reduction of the ketone is suggested to be the rate-limiting step.

As for the activation of the pre-catalyst, a stabilized van der Waals complex is observed between the catalyst and the reacting ketone during the first step of the cycle. The orientation of the molecules in this complex is favorable to the formation of the 4-center transition state (Fig. 3). Table 3 shows the relative energies, enthalpies, as well as free energies of the species involved in the first step of the catalytic cycle.

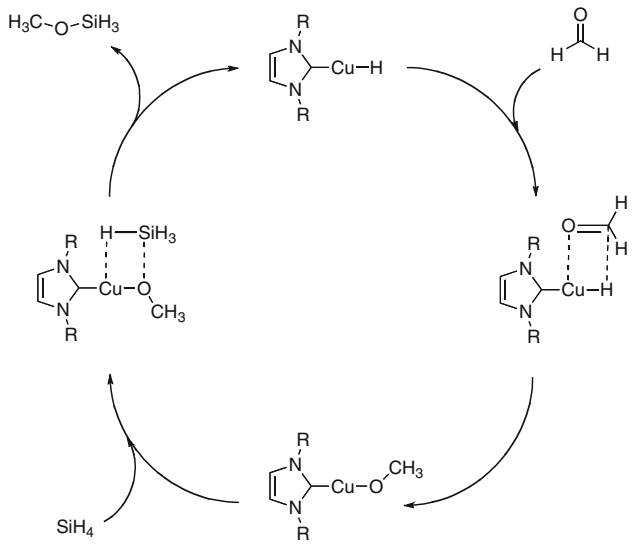

Scheme 4 The proposed mechanism for the hydrogenation of ketones by copper(I) hydride catalysts

The results show the formation of the van der Waals complex to be energetically favored by about 5 kcal/mol. The more important stabilization for NHC = ADC_H and IH complexes is not due to reduced steric effects but due to the formation of a strong hydrogen bond between the ketone oxygen atom and hydrogen atom fixed on the heterocyclic nitrogen (See Fig. 3). In true experimental systems, such interaction is not expected to occur. On the other hand, the slightly less important stabilization for the ItBu and IPr ligands can be explained by an increased steric hindrance around the copper atom.

As shown in Fig. 3, the van der Waals complexes are structurally close to the transition state, hence explaining the small energetic differences between both. At the transition state, elongated C–O and Cu–H bonds and reduced Cu–O and C–H distances characterize the complexes.

As for the activation of the pre-catalyst, the density differences at the transition state (Fig. 4) point toward an asynchronous concerted reaction mechanism, with the Cu–H–C rearrangement being more advanced than the formation of the Cu–O bond. Figure 4 shows a decrease in electron density along the Cu–H axis, as well as an increase along the H–C axis. The electron density of the C=O double bond is apparently displaced yielding a supplementary lone pair on the oxygen atom. In a second instance, the increased electronic density on the oxygen atom will be transferred to the Cu atom to complete the σ bond metathesis.

Bond indexes were, once more, calculated to give a more quantitative analysis of the transition-state asynchronicity. For this analysis, Cu–H, Cu–O, π(C–O), and C–H bonds were considered. Calculated Wiberg indexes for NHC = ADC_H, IH, and IMes are reported in Table 4.

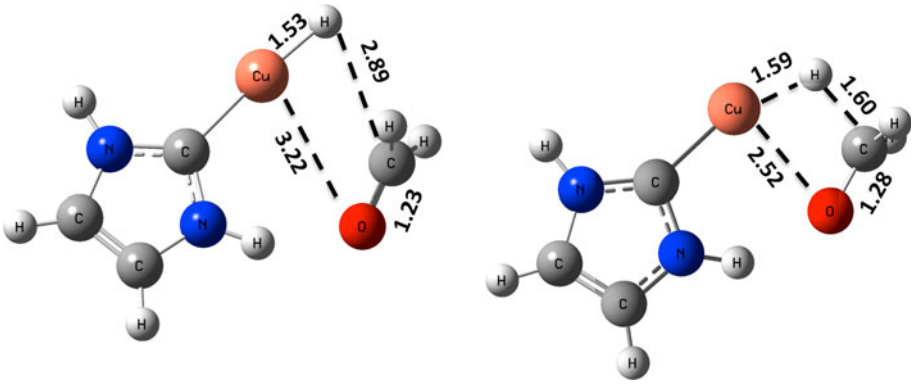

Fig. 3 Reactant van der Waals complex (*left*) and transition-state (*right*) structure for the reaction between (IH)Cu–H and H_2CO. Bond lengths are given in Å

Table 3 Relative energy ΔE, enthalpy, and free energy (ΔH; ΔG) with respect to (NHC)Cu–H and H_2CO reactants during the first step of the catalytic cycle

NHC=	van der Waals complex	TS	Products
ADC_H	−7.9 (−6.4; 3.1)	−1.8 (−0.8; 9.9)	−33.3 (−28.5; −18.8)
IH	−9.1 (−7.6; 2.3)	−2.5 (−1.6; 8.8)	−33.3 (−28.5; −18.9)
IMe	−4.9 (−3.6; 4.2)	−0.9 (−0.0; 11.2)	−33.5 (−28.7; −18.7)
IiPr	−4.9 (−3.5; 4.4)	−0.3 (0.6; 10.9)	−33.3 (−28.5; −18.9)
ItBu	−3.6 (−2.2; 5.0)	2.3 (3.2; 13.9)	−32.8 (−28.7; −18.5)
IPh	−4.9 (−3.5; 5.0)	0.4 (1.3; 12.6)	−33.5 (−28.7; −18.5)
IMes	−5.1 (−3.6; 7.4)	−0.6 (0.4; 14.5)	−33.8 (−28.9; −18.5)
IPr	−3.9 (−2.4; 7.0)	0.1 (1.0; 14.2)	−33.6 (−28.8; −19.6)

Values in kcal/mol

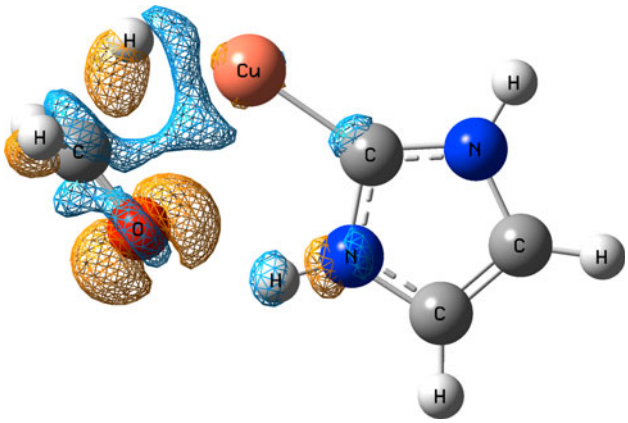

Fig. 4 Density difference between transition state and sum of reactants at transition-state geometry

According to these results, the Cu–H and π(C–O) bonds have been broken to approximately 50 % and 45 % at the TS, whereas the C–H bond has formed up to about 40–48 %. In agreement with the electronic density differences, the Cu–O bond has only been formed to a mere 4–13 %. Considering the Cu–H–C rearrangement to be more advanced than the formation of the Cu–O bond, the TS can be characterized as asynchronous, with the calculated S_y values ranged from 0.70 to 0.75. δB_{AV} average values of about 0.35 can be seen as indicative of early transition states.

For the reaction to take place, free energy barriers ranging from 9 to 15 kcal/mol with respect to the isolated reactants have to be overcome (Table 3).

As this first step of the catalytic cycle involves an electron transfer from the Cu–H bond to the ketone carbon atom, a more pronounced hydride character of the active Cu–H complex possibly explains the difference in reactivity for the different NHC ligands [76]. However, no relationship is found between the electronic population of the hydride and the free energy activation barrier $\Delta G^{\neq}$. Table S8 (in Supporting information) also confirms there to be almost no difference in charge of the hydrogen atom in the initial van der Waals complexes as NHC ligands considered in this study are similar from an electronic point of view (i.e., weak influence of the N substituents on electronic properties), and hence, this factor does not explain the difference in reactivity. However, the series of ligands considered here strongly differ from a steric point of view. To study steric effects, the "percent buried volume" ($\%V_{Bur}$) defined as the percent of the total volume of a sphere occupied by a ligand, introduced by Nolan and Cavallo [115–123], is used. To measure the $\%V_{Bur}$, we examined the DFT-optimized geometries of the free ligands by using a software developed by Cavallo et al., which is available free from charge [124, 125].[3] Table 5

[3] Optimized structures of (NHC)Cu–H complexes were transformed to *xyz* format using the Open Babel 2.3.0 program [126] keeping only the atomic coordinates of elements belonging to the NHC ligand. These were used as raw data for $\%V_{Bur}$ calculations with a distance of 2.10 Å for the metal–ligand bond. A compilation of $\%V_{Bur}$ values is presented in Table 5.

Table 4 NBO analysis for the first step of the catalytic cycle

Catalyst	Cu–H	Cu–O	C–O	C–H	δB_{AV}	S_y
(ADC_H)Cu–H						
B_i^R	0.5657	0.0221	1.7823	0.0473	0.384	0.73
B_i^{TS}	0.2629	0.0436	1.4264	0.4630		
B_i^P	0.0021	0.3267	1.0107	0.9373		
%Ev	53.73	7.06	46.12	46.71		
(IH)Cu–H						
B_i^R	0.5612	0.0302	1.7554	0.0551	0.378	0.71
B_i^{TS}	0.2655	0.0444	1.4681	0.4794		
B_i^P	0.0020	0.3245	1.0138	0.9373		
%Ev	52.88	4.83	45.42	48.1		
(IMes)Cu–H						
B_i^R	0.5523	0.0144	1.8068	0.0530	0.347	0.75
B_i^{TS}	0.2900	0.0387	1.4622	0.4002		
B_i^P	0.0018	0.3093	1.0152	0.9365		
%Ev	47.65	8.24	43.53	39.30		

Wiberg bond indexes (B_i), % evolution through the reaction coordinate ($\%E_v$), average bond index variation (δB_{AV}) ,and synchronicity parameters (S_y)

Table 5 $\%V_{Bur}$ for selected systems

Entry	NHC=	$\%V_{Bur}$
1	ADC_H	20.4
2	IH	19.4
3	IMe	25.9
4	IiPr	27.0
5	ItBu	40.8
6	IPh	33.2
7	IMes	34.4
8	IPr	42.7

shows this parameter to increase as could be expected by looking at the size of the ligand, although the overall variation is small. Larger ligands such as the IMes ligand can be characterized by lower values, highlighting the importance of the structural occupation. Strong steric hindrance is shown for ItBu and IPr ligands, as they bring crowded methyl groups in the area surrounding the Cu atom (entries 5 and 8).

Analyzing the variation in free activation energy with respect to this parameter (Fig. 5), the importance of steric hindrance on the activation barrier of the first step of the

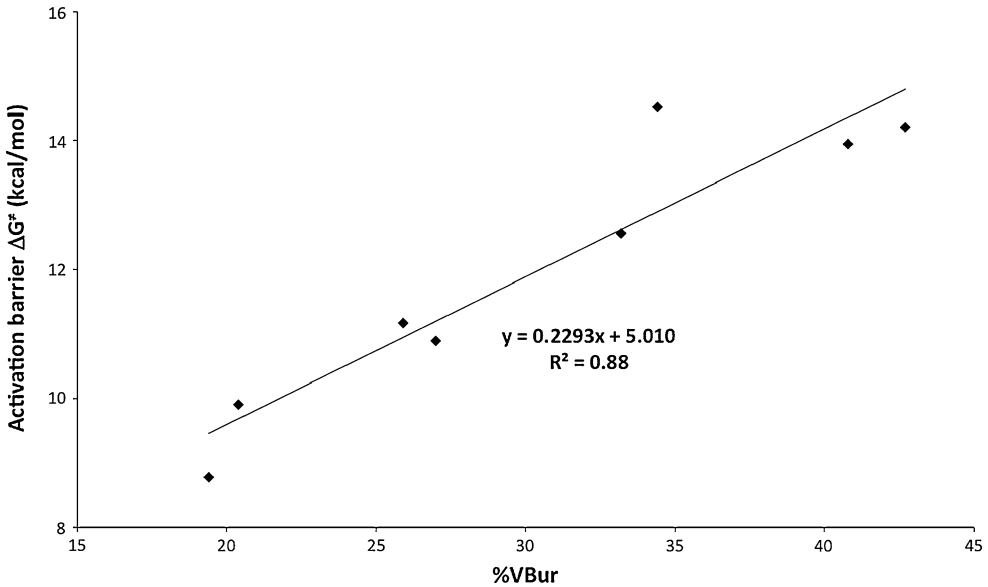

Fig. 5 Evolution of computed free activation barriers as a function of the $\%V_{Bur}$ for the first step of the catalytic cycle

Table 6 Relative energy ΔE, enthalpy, and free energy (ΔH; ΔG) with respect to (NHC)Cu–OCH_3 and SiH_4 reactants during the second step of the catalytic cycle

NHC=	van der Waals complex	TS	van der Waals complex	Products
ADC_H	−2.6 (−1.1; 8.5)	−1.0 (−0.5; 11.2)	−10.1 (−8.7; 1.6)	−5.0 (−5.0; −3.9)
IH	−2.8 (−1.3; 8.6)	−1.0 (−0.5; 9.7)	−11.2 (−9.8; 0.6)	−5.0 (−5.0; −3.8)
IMe	−2.8 (−1.3; 8.4)	−0.6 (0.1; 11.7)	−5.8 (−4.6; 3.6)	−4.8 (−4.8; −4.0)
IiPr	−2.9 (−1.4; 8.5)	−0.5 (−0.5; 13.6)	−5.7 (−4.5; 4.0)	−4.9 (−5.0; −4.6)
ItBu	−2.1 (−0.5; 9.1)	−0.9 (−0.3; 11.1)	−4.1 (−2.9; 3.4)	−5.4 (−5.5; −4.6)
IPh	−2.3 (−0.8; 8.6)	−1.0 (−1.0; 12.3)	−5.0 (−3.8; 2.3)	−4.7 (−4.8; −4.3)
IMes	−2.9 (−1.4; 8.4)	−0.1 (0.4; 13.1)	−4.8 (−3.5; 5.0)	−4.5 (−4.6; −4.2)
IPr	−2.5 (−0.8; 11.1)	0.6 (1.3; 15.6)	−4.5 (−4.5; 8.1)	−4.6 (−4.7; −3.1)

Values in kcal/mol

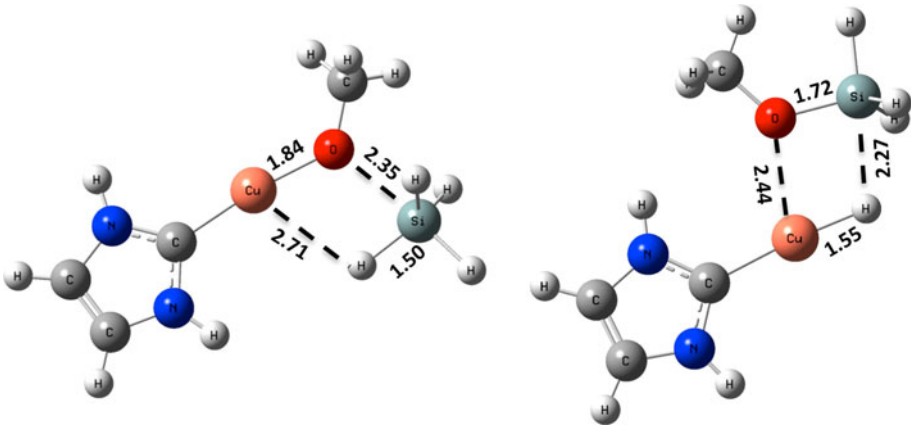

Fig. 6 Reactant van der Waals complex (*left*) and transition-state (*right*) structure for the reaction between (IH)Cu–OCH_3 and SiH_4. Bond lengths are given in Å

catalytic cycle is clearly highlighted, showing this step to be mainly under steric control.

The second step of the catalytic cycle concerns the regeneration of the catalyst, through the reaction of the Cu-alkoxide species with a silane molecule, yielding a silylated ether product. As for the previous steps, a σ metathesis reaction is suggested passing through a 4-center transition state. As for the previous steps, an energetically stabilized van der Waals complex is obtained between both compounds. The stabilizing interaction of about 3 kcal/mol (Table 6) is comparable to the energetic stabilization observed for the first step of the catalytic cycle. This interaction places the compounds in an orientation favorable to the 4-center transition state. As expected, the transition state is characterized by shortened Cu–H and Si–O bonds, and elongated SiH and Cu–O bonds, as shown in Fig. 6.

Density differences (Fig. 7) once more qualitatively show an asynchronous transition state with the Cu–O bond breaking/O–Si bond formation being more advanced compared to the hydrogen transfer toward the Cu atom. Wiberg indexes (Table 7) confirm this asynchronicity, although it being less pronounced compared to the previous steps ($S_y = 0.90$–0.95). At the TS, the Si–H and Cu–O bonds are broken at approximately 75 and 85 %, while almost 85 % of the Si–O bond has been formed. The Cu–H bond has only been formed up to about 60–65 %. δB_{AV}

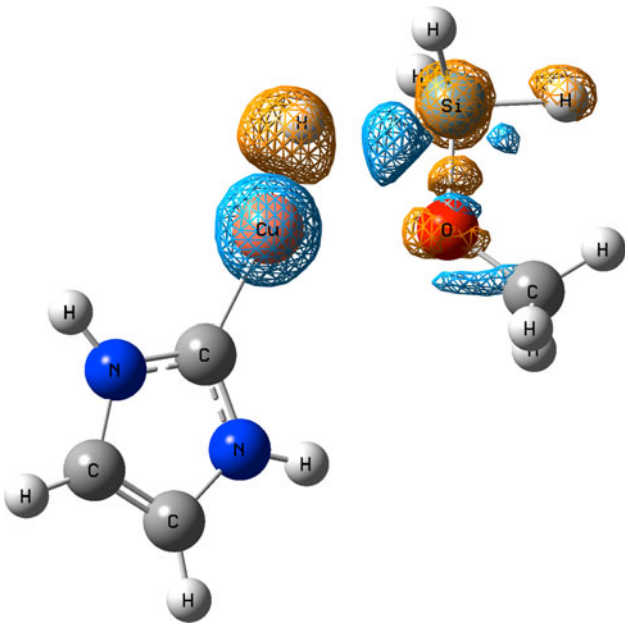

Fig. 7 Density difference between transition state and sum of reactants at transition-state geometry

average values of about 0.75 indicate late transition states, which could be anticipated from their structure as shown in Fig. 6.

For the reaction to take place, free energy barriers ranging from 9.5 to 15.5 kcal/mol have to be overcome

Table 7 NBO analysis for the second step of the catalytic cycle

Catalyst	Cu–O	Cu–H	Si–H	Si–O	δB_{AV}	S_y
(ADC_H)Cu–H						
B_i^R	0.2739	0.0056	0.9079	0.1233	0.804	0.95
B_i^{TS}	0.0407	0.4242	0.1791	0.5377		
B_i^P	0.0030	0.6140	0.0005	0.6040		
%Ev	86.08	68.80	80.32	86.21		
(IH)Cu–H						
B_i^R	0.2707	0.0056	0.9079	0.1310	0.760	0.91
B_i^{TS}	0.0334	0.3686	0.2645	0.5321		
B_i^P	0.0019	0.6158	0.0002	0.6012		
%Ev	88.28	59.49	70.88	85.30		
(IMes)Cu–H						
B_i^R	0.2614	0.0037	0.9191	0.1280	0.745	0.92
B_i^{TS}	0.0298	0.3630	0.2566	0.5355		
B_i^P	0.0012	0.6092	0.0004	0.6535		
%Ev	89.01	59.34	72.11	77.55		

Wiberg bond indexes (B_i), % evolution through the reaction coordinate ($\%E_v$), average bond index variation (δB_{AV}), and synchronicity parameters (S_y)

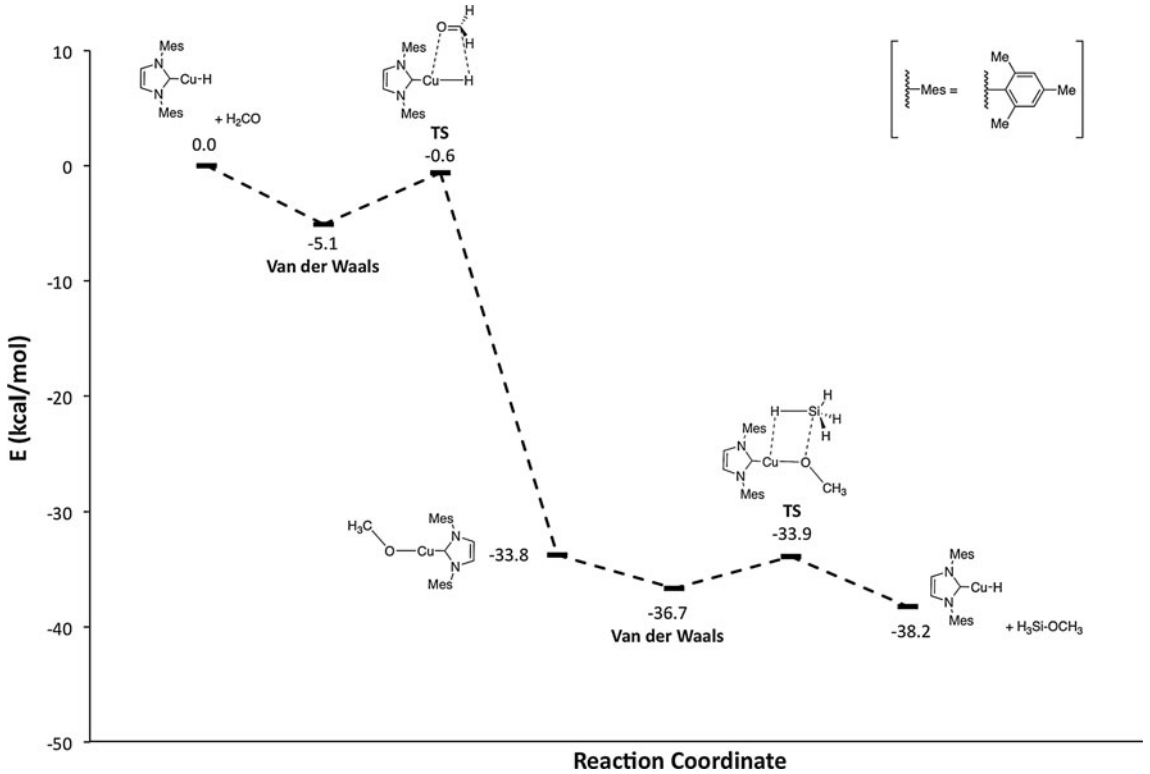

Fig. 8 Calculated B3LYP/6-31 ++G(d,p) potential energy surface (kcal/mol) for the catalytic cycle of hydrosilylation of formaldehyde by the (IMes)Cu–H catalyst

(Table 6), which are comparable to the barriers observed for the first step of the cycle (Fig. 8), and hence, the rate-determining step cannot be decided upon. Although the steric effect ($\%V_{Bur}$) once more is important, it does not explain the variation in activation barrier as well as for the first step. Other effects such as bond strength and electronic effects are likely also important to explain the differences in activation barrier.

Steric effects likely have an increasing importance for the more crowed NHC ligands, as well as for larger ketones and silanes.

Energetic barriers are, nevertheless, substantially lower than free energy barriers of 51.13 and 56.70 kcal/mol calculated for the non-catalyzed hydrosilylation of formaldehyde and acetone, respectively. The low energetic barriers calculated in this work show the plausibility of the suggested catalytic cycle and furthermore explain the high turnover number observed for these types of catalyst.

The overall catalytic cycle shows an exothermicity of about 35 kcal/mol ($\Delta H = 33.5$ kcal/mol for the (IH)Cu–H molecule), which is driven by the transformation of a πC = O bond and a σ Si–H bond into more stable σ C–H and σ O–Si bonds, and is in agreement with experimental observations.

4 Conclusions

In this paper, we have shown the theoretical validity of the suggested catalytic cycle for the hydrosilylation of ketones using N-heterocyclic diaminocarbenes Cu(I) hydride catalysts. The activation of the catalyst from a copper fluoride complex, as well as both steps of the catalytic cycle, involves a 4-center σ metathesis transition state. The reactants are guided toward these transition states, through the formation of energetically favored van der Waals complexes, formed through favorable electrostatic interactions. Analysis of transition states shows that the σ metathesis reactions studied here can be described as asynchronous concerted mechanisms, with the transfer from Cu-linked atoms occurring prior to the transfer toward the metal center.

For the reductive hydrosilylation of a ketone by SiH_4 to take place, a free energy barrier of about 14 kcal/mol (for the more realistic ItBu, IMes, and IPr models) with respect to the isolated reactants has to be overcome. Comparable energy barriers are obtained for the two successive steps of the catalytic cycle, not allowing to identify a rate-limiting step, if there should be one.

Finally, we noted an overall exothermicity of the catalytic cycle of about 35 kcal/mol, driven by the transformation of a πC = O bond and a σ Si–H bond into more stable σ C–H and σ O–Si bonds.

Acknowledgments The authors would like to thank the Université Catholique de Louvain (Thomas Vergote is a UCL research assistant). They would also like to thank the Fond de la Recherche Scientifique de Belgique (FRS-FNRS) for funding computational resources provided by the supercomputing facilities of the Université Catholique de Louvain (CISM/UCL) and the Consortium des Equipements de Calcul Intensif en Fédération Wallonie-Bruxelles (CECI).

References

1. Smith MB, March J (2001) March's advanced organic chemistry. Wiley, New York
2. Ohkuma T, Noyori R (1999) Hydrogenation of carbonyl groups. In: Jacobsen EN, Pfaltz A, Yamamoto H (eds) Comprehensive asymmetric catalysis. Springer, Berlin, pp 199–246
3. Nishiyama H, Itoh K (2000) Asymmetric hydrosilylation and related reactions. In: Ojima I (ed) Catalytic asymmetric synthesis. Wiley, New York, pp 111–144
4. Corey EJ, Helal CJ (1998) Angew Chem Int Ed 37:1986–2012
5. Marciniec B, Maciejewski H, Pietraszuk C, Pawluć P (2009) Advances in silicon science, vol 1: hydrosilylation a comprehensive review on recent advances. Springer, Berlin
6. Ojima I, Nihonyanagi M, Nagai Y (1972) J Chem Soc Chem Commun 1972:938–938
7. Langlois N, Dang TP, Kagan HB (1973) Tetrahedron Lett 49: 4865–4868
8. Dumont W, Poulin J-C, Kagan HB (1973) J Am Chem Soc 95:8295–8299
9. Du G, Abu-Omar MM (2006) Organometallics 25:4920–4923
10. Ison EA, Trivedi ER, Corbin RA, Abu-Omar MM (2005) J Am Chem Soc 127:15374–15375
11. Nolin KA, Krumper JR, Pluth MD, Bergman RG, Toste FD (2007) J Am Chem Soc 129:14684–14696
12. Gade LH, Cesar V, Bellemin-Laponnaz S (2004) Angew Chem Int Ed 43:1014–1017
13. Nishiyama H, Sakaguchi H, Nakamura T, Horihata M, Kondo M, Itoh K (1989) Organometallics 8:846–848
14. Tao B, Fu GC (2002) Angew Chem Int Ed 41:3892–3894
15. Sawamura M, Ryoichi K, Ito Y (1994) Angew Chem Int Ed 33: 111–113
16. Zhu G, Terry M, Zhang X (1997) J Organomet Chem 547: 97–101
17. Nishibayashi Y, Takei I, Uemura S (1998) Organometallics 17:3420–3422
18. Chianese AR, Crabtree RH (2005) Organometallics 25:3066–3073
19. Nakano T, Nagai Y (1988) Chem Lett 17:481–484
20. Carter MB, SchiØtt B, Gutiérrez A, Buchwald SL (1994) J Am Chem Soc 116:11667–11670
21. Halterman R, Ramsey TM, Chen Z (1994) J Org Chem 59: 2642–2644
22. Xin S, Harrod JF (1995) Can J Chem 73:999–1002
23. Bandini M, Bernardi F, Bottoni A, Cozzi PG, Miscione GP, Umani-Ronchi A (2003) Eur J Org Chem 2003:2972–2984
24. Imma H, Mori M, Nakai T (1996) Syn Lett 1996:1229–1230
25. Mandini M, Cozzi PG, Nego L, Umani-Ronchi A (1999) Chem Comm 1999:39–40
26. Yun J, Buchwald SL (1999) J Am Chem Soc 121:5640–5644
27. Brunner H, Fisch K (1990) Angew Chem Int Ed 29:1131–1132
28. Shaikh NS, Enthaler S, Junge K, Beller M (2008) Angew Chem Int Ed 47:2497–2501
29. Langlotz BK, Wadepohl H, Gade LH (2008) Angew Chem Int Ed 41:4670–4674
30. Son SU, Paik S-J, Lee IS, Lee Y-A, Chung YK (1999) Organometallics 18:4114–4118
31. DiBiase Cavanaugh M, Gregg BT, Cutler AR (1996) Organometallics 15:2764–2769
32. Mimoun H, de Saint Laumer JY, Giannini L, Scopelliti R, Floriani C, Am J (1999) Chem Soc 121:6158–6166
33. Mimoun H (1999) J Org Chem 64:2582–2589
34. Ohkuma T, Hashiguchi S, Noyori R (1994) J Org Chem 59: 217–221

35. Bette V, Mortreux A, Savoia D, Carpentier J-F (2004) Tetrahedron 60:2837–2842
36. Brunner H, Miehling W (1984) J Organomet Chem 275:C17–C21
37. Lipshutz BH, Chrisman W, Noson K (2001) J Organomet Chem 624:367–371
38. Wu J, Ji J-X, Chan ASC (2005) Proc Nat Acad Sci 102: 3570–3575
39. Lee D-W, Yun J (2004) Tetrahedron Lett 45:5415–5417
40. Issenhuth JT, Dagorne S, Bellemin-Laponnaz S (2006) Adv Synth Catal 348:1991–1994
41. Riant O, Mostefaï N, Courmarcel J (2004) Synthesis 18:2943–2958
42. Lipshutz BH (2002) Copper(I)-mediated 1,2- and 1,4-Reductions. In: Krause N (ed) Modern organocopper chemistry. Wiley-VCH, Weinheim, pp 167–187
43. Riant O (2009) Copper(I) hydride reagents and catalysts. In: Rappoport Z, Marek I (ed) The chemistry of organocopper compounds. Wiley, pp 731–773
44. Lipshutz BH, Noson K, Chrisman W (2001) J Am Chem Soc 123:12917–12918
45. Lipshutz BH, Lower A, Noson K (2002) Org Lett 4:4045–4048
46. Lipshutz BH, Caires CC, Kuipers P, Chrisman W (2003) Org Lett 5:3085–3088
47. Lipshutz BH, Frieman BA (2005) Angew Chem 117:6503–6506
48. Lipshutz BH, Frieman BA (2005) Angew Chem Int Ed 44:6345–6348
49. Czekelius C, Carreira EM (2004) Org Lett 6:4575–4578
50. Sirol S, Courmarcel J, Mostefaï N, Riant O (2001) Org Lett 3: 4111–4113
51. Courmarcel J, Mostefaï N, Sirol S, Choppin S, Riant O (2001) Isr J Chem 41:231–240
52. Mostefaï N, Sirol S, Courmarcel J, Riant O (2007) Synthesis 8:1265–1271
53. Yu F, Zhou JN, Zhang XC, Sui YZ, Wu FF, Xie LJ, Chan ASC, Wu J (2011) Chem Eur J 17:14234–14240
54. Díez-González S, Nolan SP (2005) Annu Rep Prog Chem Sect B 101:171–191
55. Herrmann WA (2002) Angew Chem Int Ed 41:2162–2187
56. Bourissou D, Guerret O, Gabbai FP, Bertrand G (2000) Chem Rev 100:39–91
57. Arduengo AJ III (1999) Acc Chem Res 32:913–921
58. Arduengo AJ III, Harlow RL, Kline M (1991) J Am Chem Soc 113:361–363
59. Navarro O, Kelly RA III, Nolan SP (2003) J Am Chem Soc 125:16194–16195
60. Viciu MS, Germaneau RF, Nolan SP (2002) Org Lett 4: 4053–4056
61. Lee CW, Choi T-L, Grubbs RH (2002) J Am Chem Soc 124: 3224–3225
62. Herrmann WA, Bohm VPW, Gstottmayr CWK, Grosche M, Reisinger CP, Weskamp TJ (1999) Organomet Chem 586: 563–565
63. Kaur H, Zinn FK, Stevens ED, Nolan SP (2004) Organometallics 23:1157–1160
64. Díez-González S, Kaur H, Zinn FK, Stevens ED, Nolan SP (2005) J Org Chem 70:4784–4796
65. Yun J, Kim D, Yun H (2005) Chem Comm 2005:5181–5183
66. Díez-González S, Scott NM, Nolan SP (2006) Organometallics 25:2355–2358
67. Díez-González S, Stevens ED, Scott NM, Petersen JL, Nolan SP (2008) Chem Eur J 14:158–168
68. Vergote T, Nahra F, Welle A, Luhmer M, Wouters J, Mager N, Riant O, Leyssens T (2012) Chem Eur J 18:793–798
69. Albright A, Gawley RE (2011) J Am Chem Soc 133:19680–19683
70. Díez-González S, Nolan SP (2008) Acc Chem Res 41:349–358
71. Díez-González S, Nolan SP (2008) Aldrichimica Acta 41:43–51
72. Ito H, Ishizuka T, Okumura T, Yamanaka H, Tateiwa J-I, Sonoda M, Hosomi A (1999) J Organomet Chem 574:102–106
73. Mankad NP, Laitar DS, Sadighi JP (2004) Organometallics 23:3369–3371
74. Gathy T, Peeters D, Leyssens T (2009) J Organomet Chem 694: 3943–3950
75. Gathy T, Leyssens T, Peeters D (2011) Comp Theor Chem 970: 23–29
76. Gathy T, Riant O, Peeters D, Leyssens T (2011) J Organomet Chem 696:3425–3430
77. Issenhuth J-T, Notter F-P, Dagorne S, Dedieu A, Bellemin-Laponnaz S (2010) Eur J Inorg Chem 2010:529–541
78. Zhang W, Li W, Qin S (2012) Org Biomol Chem 10:597–604
79. Becke AD (1993) J Chem Phys 98:5648–5653
80. Lee C, Yang W, Parr RG (1988) Phys Rev B37:785–789
81. Frisch MJ, Trucks GW, Schlegel HB, Scuseria GE, Robb MA, Cheeseman JR, Montgomery JA Jr, Vreven T, Kudin KN, Burant JC, Millam JM, Iyengar SS, Tomasi J, Barone V, Mennucci B, Cossi M, Scalmani G, Rega N, Petersson GA, Nakatsuji H, Hada M, Ehara M, Toyota K, Fukuda R, Hasegawa J, Ishida M, Nakajima T, Honda Y, Kitao O, Nakai H, Klene M, Li X, Knox JE, Hratchian HP, Cross JB, Bakken V, Adamo C, Jaramillo J, Gomperts R, Stratmann RE, Yazyev O, Austin AJ, Cammi R, Pomelli C, Ochterski JW, Ayala PY, Morokuma K, Voth GA, Salvador P, Dannenberg JJ, Zakrzewski VG, Dapprich S, Daniels AD, Strain MC, Farkas O, Malick DK, Rabuck AD, Raghavachari K, Foresman JB, Ortiz JV, Cui Q, Baboul AG, Clifford S, Cioslowski J, Stefanov BB, Liu G, Liashenko A, Piskorz P, Komaromi I, Martin RL, Fox DJ, Keith T, Al-Laham MA, Peng CY, Nanayakkara A, Challacombe M, Gill PMW, Johnson B, Chen W, Wong MW, Gonzalez C, Pople JA (2004) Gaussian 03, revision C.02. Gaussian, Wallingford
82. Fukui K (1970) J Phys Chem 74:4163–6161
83. Fukui K (1981) Acc Chem Res 14:363–368
84. Gonzalez C, Schlegel HB (1989) J Chem Phys 90:2154–2161
85. Gonzalez C, Schlegel HB (1990) J Phys Chem 94:5523–5527
86. Grimme S, Antony J, Ehrlich S, Krieg H (2010) J Chem Phys 132:154104–154123
87. Hay PJ, Wadt WR (1985) J Chem Phys 82:270–283
88. Hay PJ, Wadt WR (1985) J Chem Phys 82:284–298
89. Hay PJ, Wadt WR (1985) J Chem Phys 82:299–310
90. Hehre WJ, Ditchfield R, Pople JA (1972) J Chem Phys 56:2257–2261
91. Hariharan PC, Pople JA (1973) Theor Chim Acta 28:213–222
92. Foster JP, Weinhold F (1980) J Am Chem Soc 102:7211–7218
93. Reed AE, Weinhold F (1983) J Chem Phys 78:4066–4073
94. Reed AE, Weinstock RB, Weinhold F (1985) J Chem Phys 83: 735–746
95. Reed AE, Weinhold F (1985) J Chem Phys 83:1736–1740
96. Keith T, Millam J (2006) Gaussview, version 4.1.2, R. Dennington, II, Semichem, Inc., Shawnee
97. Weigend F, Ahlrichs R (2005) Phys Chem Chem Phys 7:3297–3305
98. Perdew JP (1986) Phys Rev B 33:8822–8824
99. Becke AD (1988) Phys Rev A 38:3098–3100
100. Perdew JP (1991) Beyond the local density approximation. In: Ziesche P, Esching H (eds) Electronic structure of solids '91. Akademie Verlag, Berlin, pp 11–20
101. Adamo C, Barone V (1998) J Chem Phys 108:664–675
102. Quintal MM, Karton A, Iron MA, Boese AD, Martin JML (2006) J Phys Chem 110:709–716
103. Sousa SF, Fernandes PA, Ramos MJ (2007) J Phys Chem A 111: 10439–10452
104. Schultz NE, Zhao Y, Truhlar DG (2005) J Phys Chem A 109: 11127–11143

105. Roy LE, Hay PJ, Martin RL (2008) J Chem Theory Comput 4: 1029–1031
106. Ehlers AW, Bihme M, Dapprich S, Gobbi A, Hollwaerth A, Jonas V, Kokler KF, Stegmann R, Veldkamp A, Frenking G (1993) Chem Phys Lett 208:111–114
107. Bergner A, Dolg M, Kuechle W, Stoll H, Preuss H (1993) Mol Phys 80:1431–1441
108. Kaupp M, Schleyer PVR, Stoll H, Preuss H (1991) J Chem Phys 94:1360–1366
109. Dolg M, Stoll H, Preuss H, Pitzer RM (1993) J Phys Chem 97: 5852–5859
110. Mahonney WS, Bretensky DM, Stryker JM (1988) J Organomet Chem 110:291–294
111. Wiberg K (1968) Tetrahedron 24:1083–1096
112. Moyano A, Pericas M, Valenti E (1989) J Org Chem 54: 573–582
113. Lecea B, Arrieta A, Roa G, Ugalde J, Cossio F (1994) J Am Chem Soc 116:9613–9619
114. Heredia MM, Lorono M, Cordova T, Chuchani G (2005) J Mol Struct: Theochem 770:131–137
115. Cavallo L, Correa A, Costabille C, Jacobsen H (2005) J Organomet Chem 690:5407–5413
116. Hillier AC, Sommer WJ, Yong BS, Petersen JL, Cavallo L, Nolan SP (2003) Organometallics 22:4322–4326
117. Bazinet P, Ong T-G, O'Brien JS, Lavoie N, Bell E, Yap GPA, Korobkov I, Richeson DS (2007) Organometallics 26:2885–2895
118. Fortman GC, Scott NM, Linden A, Stevens ED, Dorta R, Nolan SP (2010) Chem Comm 46:1050–1052
119. Clavier H, Correa A, cavallo L, Escuerdo-Adán EC, Benet-Buchholz J, Slawin AMZ, Nolan SP (2009) Eur J Inorg Chem 2009:1767–1773
120. Viciu MS, Navarro O, Germaneau RF, Kelly RA III, Sommer W, Marion N, Stevens ED, Cavallo L, Nolan SP (2004) Organometallics 23:1629–1635
121. Dorta R, Stevens ED, Scott NM, Costabile C, Cavallo L, Hoff CD, Nolan SP (2005) J Am Chem Soc 127:2485–2495
122. Kelly RA III, Clavier H, Giudice S, Scott NM, Stevens ED, Bordner J, Samardjiev I, Hoff CD, Cavallo L, Nolan SP (2008) Organometallics 27:202–221
123. Urbina-Blanco CA, Bantreil X, Clavier H, Slawin AMZ, Nolan SP (2010) Beilstein J Org Chem 6:1120–1126
124. Poater A, Cosenza B, Correa A, Giudice S, Ragone F, Scarano V, Cavallo L (2009) Eur J Inorg Chem 2009:1759–1766
125. http://www.molnac.unisa.it/OMtools/sambvca.php
126. Available free of charge at: http://openbabel.sourceforge.net